Mapping Bragg Scatter with a Polarimetric WSR-88D

VALERY M. MELNIKOV

Cooperative Institute for Mesoscale Meteorological Studies, University of Oklahoma, Norman, Oklahoma

RICHARD J. DOVIAK, DUSAN S. ZRNIĆ, AND DAVID. J. STENSRUD

NOAA/OAR/National Severe Storms Laboratory, Norman, Oklahoma

(Manuscript received 16 December 2010, in final form 5 May 2011)

ABSTRACT

Using a polarimetric Weather Surveillance Radar-1988 Doppler (WSR-88D) radar to distinguish Bragg scatterers from insects and birds in an optically clear atmosphere has the potential to provide information on convective boundary layer depth. Measured median differential reflectivities Z_{DR} of Bragg scatterers lie between −0.08 and 0.06 dB, which supports the hypothesis that the intrinsic Z_{DR} of Bragg scatters is 0 dB. Thus, the intrinsic 0 dB of Bragg scatter can be used for verifying of Z_{DR} radar calibration. Measured copolar correlation coefficients ρ_{hv} have distributions peaked at about 0.998–1.0. If insects and birds are spatially separated from Bragg scatterers, the dual-polarization capability of the WSR-88D allows distinguishing echoes from these two types of scatterers since Z_{DR} from biota is significantly larger than 0 dB. In mixtures of Bragg and biota scatter, polarimetric spectral analysis shows differences in portions of the H and V spectra where birds and insects could be contaminating echoes from Bragg scatterers.

The values of $Z_{DR} \approx 0$ and $\rho_{hv} \approx 1$ that characterize Bragg scatterers allow coherent summation of signals from the H and V receiver channels and restoration of measurement capability lost as a result of splitting power into H and V channels. Further enhancements to data collection and signal processing allow power measurement, with a standard deviation of about 1 dB, of weak echoes from Bragg scatterers having equivalent reflectivity factors of about −28 dBZ at distance of 10 km from the radar. This level of reflectivity corresponds to a refractive index structure parameter C_n^2 of about 4×10^{-15} m$^{-2/3}$, a typical magnitude found in maritime air.

1. Introduction

Forecasting the time and location of storms requires knowledge of the water vapor field in the convective boundary layer (CBL; e.g., National Research Council 1998). Rawinsondes twice a day at stations 500 km apart are not often or dense enough to reliably provide useful information for storm prediction models in situations having rapidly changing atmospheric conditions. Water vapor measurements from radiometers (e.g., Ulaby et al. 1986) on the ground or in space do not have the required height and/or temporal resolution to be consistently useful for ingestion into numerical storm prediction models. Water vapor is the strongest contributor to the lower atmosphere's refractive index and, given the initial pressure, temperature, and water vapor fields, changes in refractive index, and by proxy water vapor, near the ground can be monitored using radar measurements of changes in the phase path between the radar and stationary ground objects (Fabry et al. 1997; Fabry 2006; Heinselman et al. 2009b; Bodine et al. 2010). By measuring the phase path change to a wide distribution of ground objects, water vapor changes have been monitored with about 4-km horizontal and 4–10-min temporal resolutions (Roberts et al. 2008). This phase path method provides spatial and temporal changes in the horizontal distribution of the refractivity field and water vapor in the lowest regions of the atmosphere to ranges of about 30 km. But this method does not reveal the height profile of either refractivity or water vapor. Even within well-mixed CBLs, Mahrt (1977) shows that water vapor can decrease rapidly with height. A technique that provides an estimate of the CBL depth and information on the water vapor

Corresponding author address: Valery M. Melnikov, Cooperative Institute for Mesoscale Meteorological Studies, University of Oklahoma, 120 David L. Boren Blvd., Norman, OK 73072.
E-mail: valery.melnikov@noaa.gov

DOI: 10.1175/JTECH-D-10-05048.1

content would benefit forecasters and improve the initial conditions of numerical weather prediction models.

Bragg backscatter from refractive index perturbations $\Delta N(\mathbf{r}, t)$, at scales half the centimetric and metric wavelengths of atmospheric radars, return sufficient energy to be useful in measuring wind and the refractive index structure parameter C_n^2, a parameter proportional to reflectivity η (e.g., Hardy et al. 1966; Gossard and Strauch 1983; Doviak and Zrnic 2006, their chapter 11). As with the phase path measurements, water vapor perturbations in the CBL are the strongest contributor to C_n^2. But unlike phase path measurements, C_n^2 is strongly dependent on turbulent mixing in gradients of mean potential refractive index (Ottersen 1969; Doviak and Zrnic 2006, their section 11.6); these gradients are typically strongest at boundaries of water vapor layers. For example, large values of C_n^2 typically occur at the top of the CBL (e.g., Wyngaard and LeMone 1980; Fairall 1991; Doviak and Zrnic 2006, their section 11.7) where there is strong mixing of moist and dry air. Heinselman et al. (2009a) show if the reflectivity field obtained with the WSR-88D exhibits an elevated maximum, its height correlates well with the top of the CBL. Because insects and birds contaminate radar measurements of CBL properties, a potentially more reliable indicator of CBL depth is Bragg scatter from refractive index perturbations.

In absence of echoes from atmospheric biota, radar wind profilers measure height profiles of C_n^2 above their sites but they do not map the horizontal structure of this parameter. If there are many biotic scatterers within the resolution volume, profilers cannot distinguish C_n^2 from reflectivity due to biota. Migrating birds and insects cause problems with interpretation of data from radar wind profiler (Wilczak et al. 1995) and Weather Surveillance Radar-1988 Doppler (WSR-88D) wind measurements (e.g., Wilson et al. 1994; Bachmann and Zrnic 2007; Holleman et al. 2008). However, the scanning polarimetric WSR-88D has the capability to distinguish echoes from atmospheric biota and Bragg scatterers and thus the potential to provide information on the temporal and spatial structure of C_n^2. Thus, the main goal of our study is to determine the polarimetric properties of Bragg scatter associated with refractive index perturbations; these properties are reported on in section 4.

2. KOUN data collection and signal processing enhancements to map weak echoes

In "clear air" situations, the network WSR-88Ds operate in the 4.5-μs long-pulse mode to gain up to a 9.5-dB increase in SNR so that winds in weakly scattering regions can be measured. This large increase in SNR is only obtained if the resolution volume is filled. Although the signal-to-noise ratio (SNR) improves using the long-pulse mode, a problem in resolving thin layers of Bragg scatter is this mode's coarse-range resolution of $\sigma_r = 0.35c\tau/2 = 236$ m [c is speed of light and τ is the transmitted pulse length; Doviak and Zrnic 2006, their Eq. (5.76)]. At higher elevation angles, in particular, this coarse-range resolution acts to coarsen the height resolution. Furthermore, to make quantitative measurements of C_n^2, the dimensions of the resolution volume must be smaller than the outer scale of inertial subrange turbulence (Ottersen 1969; Gage et al. 1980; Gossard and Strauch 1983), which is in interval 10–200 m so that the long-pulse resolution is much larger than the outer scale. Thus, we have chosen to collect data in the 1.57-μs short-pulse mode, which yields a range resolution of 82 m.

For a 0.93° one-way 3-dB beamwidth of KOUN (i.e., NSSL's polarimetric WSR-88D located in Norman, Oklahoma), we have chosen to specify angular resolutions in terms of the second central moments (i.e., σ_θ^2) of the angular weighting function (Doviak and Zrnic 2006, their section 5.2). For KOUN, the two-way angular resolution is $\sigma_\theta = 0.28°$ so that at a range of 17 km, the beam has a transversal size that matches the range resolution.

To enhance detectability of weak echoes and to reduce parameter estimate variance at low SNR, the following data collection and signal processing procedures were implemented on KOUN:

1) Increased the dwell time (i.e., 0.1 s, yielding 128 samples at the pulse repetition frequency of 1280 Hz).
2) Collected data at smaller elevation increments (i.e., 0.25°).
3) Doubled the range sampling rate.
4) Implemented a two-dimensional noise speckle remover to reduce the occurrence of false echoes as in Melnikov and Schlatter (2011).
5) Used covariance products to estimate differential reflectivity Z_{DR} and the correlation coefficient ρ_{hv} as in Melnikov and Zrnic (2007).
6) Collected data in vertical scans to elevations higher than 20° to better resolve and interpret the fine details of reflectivity layers at close range.
7) Implemented ground clutter filtering at all elevation angles.
8) Coherently summed signals from the horizontal (H) and vertical (V) channels.

These procedures improved data presentations to better show the fine details of the vertical structure and polarimetric properties of clear-air scattering layers as viewed on range–height indicator (RHI) displays. To complete one vertical scan from 0° to 50°, 20 s are needed.

The U.S. National Weather Service is upgrading the WSR-88D network with polarimetric capabilities.

TABLE 1. The Z_{10} (dBZ) and C_{n10}^2 ($m^{-2/3}$) to achieve the indicated SNR at a 10-km range.

Polarization	Z_{10} (dBZ)	$C_{n10}^2(m^{-2/3})$
Single (legacy WSR-88D) (M = 66; SNR = 0 dB)	−21.5	1.8×10^{-14}
Dual (M = 66; SNR= 2 dB)	−16.5	5.6×10^{-14}
Dual (enhanced processing) (M = 768; SNR = −7 dB)	−25.5	7.1×10^{-15}
Dual, (coherently combining dual polarization data)* (M = 768; SNR = −7 dB)	−28.5	3.5×10^{-15}

* Entry applies assuming Z_{DR} = 0 dB and ρ_{hv} = 1.0.

Table 1 compares reflectivity, Z_{10}, (and C_{n10}^2) required for the WSR-88D (i.e., with M number of samples) to obtain a specified per pulse SNR for echoes from scatterers at a 10-km range. SNR values are chosen to substantially reduce speckle in reflectivity displays, but can also be chosen based on specified accuracy of polarimetric measurements. Comparison is made at a range of 10 km, the reference distance often used in specifying the performance of cloud radars (e.g., Moran et al. 1998; Melnikov et al. 2011). For the legacy WSR-88D transmitting waves having single polarization, Z_{10} = −21.5 dBZ (Doviak and Zrnic 2006, their Table 3.1); this is the first entry in Table 1.

Operation in a dual-polarization mode without any changes in the WSR-88D data collection and signal processing procedures produces the second entry in Table 1. This mode has transmitted power shared equally in horizontally and vertically polarized waves that are simultaneously radiated and simultaneously received (Doviak et al. 2000). A SNR of +2 dB is that used operationally to substantially reduce speckle in the reflectivity displays. These conditions cause a 5-dB higher Z_{10} than for the single polarization mode.

An equivalent number of samples for the enhanced processing is M = 768 [i.e., 128 time samples in each dwell time, multiplied by the number (i.e., 4) of dwell times in each 1° of elevation angle, times 1.5, which is the effective variance reduction factor associated with averaging reflectivity estimates from 2 contiguous resolution volumes separated by 125 m]. The noise speckle filter removes practically all speckles at SNR = −7 dB, so this threshold was used in our radar observations. This is the third entry in Table 1. The standard deviation of reflectivity and differential reflectivity, with M = 768 and SNR = −7 dB, is about 1 dB (Fig. 1). Coherently summing (section 2a) the signals from the H and V channels further reduces the required Z_{10}; this is the last entry in Table 1.

By combining expressions for Z and reflectivity η of Bragg scatterers [e.g., Eqs. (4.31) and (11.104) in Doviak and Zrnic (2006)], $\log_{10}[C_n^2\ (m^{-2/3})]$ can be expressed in terms of Z (dBZ) as

$$\log_{10}[C_n^2(m^{-2/3})] = 0.1Z(\text{dB}Z) - 11.6. \qquad (1)$$

Minimal C_{n10}^2 at 10 km corresponding to Z_{10} is also shown in Table 1. If enhanced processing is used, the minimal

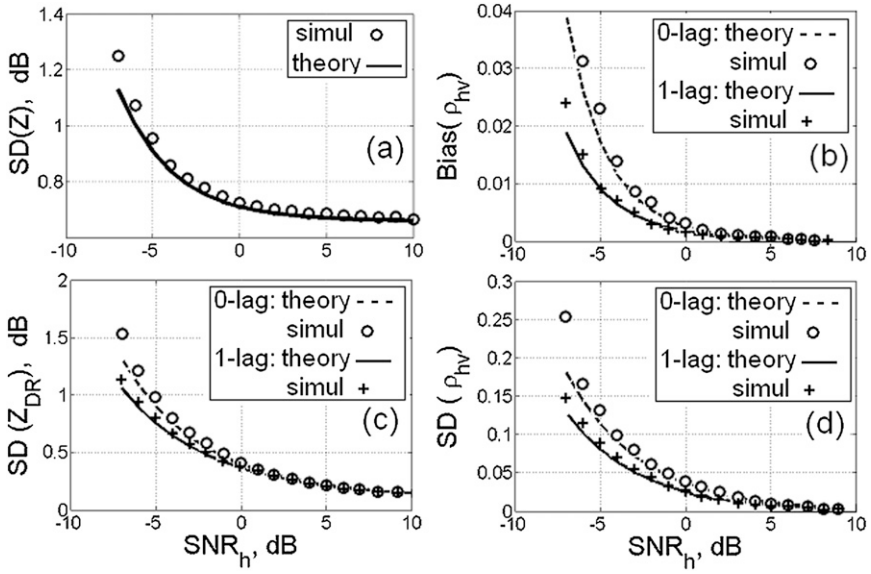

FIG. 1. Statistical properties of polarimetric variables obtained from simulations (plotted circles and pluses) and theory (curves) for λ = 10 cm, PRF = 1280 Hz, σ_v = 1 m s^{-1}, and M = 768. (a) SD(Z), (b) bias of ρ_{hv} estimates using lag 0 and lag 1 data, (c) SD(Z_{DR}), and (d) SD(ρ_{hv}).

C_{n10}^2 is 3.5×10^{-15} m$^{-2/3}$. This level is more than two orders of magnitude below the mean C_n^2 value of 5×10^{-13} m$^{-2/3}$ measured with radar and an airborne refractometer in maritime boundary layer air over Oklahoma (Doviak and Berger 1980).

The limit of radar sensitivity for KOUN can be demonstrated with Fig. 3a (we discuss this figure in detail later) where at distances near 10 km, minimal $\log(C_n^2)$ are in interval -14 to -14.1. These figures correspond to C_n^2 in interval 1.0×10^{-14} to 8×10^{-15} m$^{-2/3}$. Standard deviations of Z and the polarimetric parameter estimates as a function of SNR for $M = 768$, $\rho_{hv} = 0.998$, $Z_{DR} = 0$ dB, parameter values that appear to characterize Bragg scatter properties (section 4), are shown in Fig. 1. Results from theory (Melnikov and Zrnic 2007) and simulation agree, and SD(Z) is less than 1.5 dB for SNR ≥ -7 dB and $\sigma_v = 1$ m s^{-1}. These accuracies should be sufficient to obtain meaningful maps of weak reflectivity fields.

a. Further enhancement to weak signal measurement capability

Because Bragg scatter H and V signals have $\rho_{hv} \approx 1$ (section 4), the coherent summation of these signals can increase the Bragg scatter measurement capability. The sum of voltages e in the H and V channels is

$$e_{sum} = e_h + e_v = s_h + n_h + s_v + n_v, \qquad (2)$$

where s and n are weather and noise voltages, respectively. The mean power of the sum signal is

$$P_{sum} = \langle e_{sum} e_{sum}^* \rangle = S_h + S_h + \langle s_h^* s_v \rangle + \langle s_h s_v^* \rangle + N_h + N_v$$

Here S_h, S_v, and N_h, N_v are signal and noise powers, respectively; the brackets define ensemble (or time) averages; and the asterisk denotes complex conjugate. There are no cross terms of signal and noise because weather signal and noise voltages are zero mean and are uncorrelated. Equation (2) then can be written as

$$P_{sum} = S_h + S_h + 2(S_h S_v)^{1/2} \rho_{hv} \cos(\phi_{DP}) + N_h + N_v. \qquad (3)$$

Since there is no differential phase shift for propagation if the dominant scattering mechanism is isotropic Bragg scatter, the measured differential phase φ_{DP} equals the known system differential phase.

The summed signal SNR is

$$\frac{S_{sum}}{N_{sum}} = \frac{S_h + S_v + 2(S_h S_v)^{1/2} \rho_{hv} \cos(\phi_{DP})}{N_h + N_v}. \qquad (4)$$

By digitally multiplying the signal in H channel by $\exp(j\varphi_{DP})$ before summation, the phase of the H signal is shifted to be the same as the V signal phase; this shift effectively makes $\varphi_{DP} = 0$ in (4). For equal noise powers (i.e., $N_h = N_v = N$), (4) can be written in terms of the scatterer's differential reflectivity, $Z_{dr} = S_h/S_v$, as

$$\frac{S_{sum}}{N_{sum}} = \frac{1}{2}(1 + Z_{dr} + 2Z_{dr}^{1/2} \rho_{hv}) \frac{S_v}{N}, \qquad (5a)$$

or, in terms of S_h/N,

$$\frac{S_{sum}}{N_{sum}} = \frac{1}{2}(1 + Z_{dr}^{-1} + 2Z_{dr}^{-1/2} \rho_{hv}) \frac{S_h}{N}. \qquad (5b)$$

Because $Z_{dr} \approx 1$ and $\rho_{hv} \approx 1$ for Bragg scatter (section 4), $S_{sum}/N_{sum} = 2S_h/N = 2S_v/N$. In other words, coherent summation restores, for observations of echoes from Bragg scatterers, the loss of sensitivity caused by splitting the transmitted power into the H and V fields as done in KOUN. An example of the spatial expansion of data fields, due to the S/N increase after coherent summation, can be seen by comparing Figs. 2a,b. Although the increase in data area is minimal, there can be significant improvement in the accuracy of measurement as can be deduced from Fig. 1. This improves the KOUN capability to observe weak echoes and make accurate measurement of meteorological parameters using echoes from Bragg scatterers.

b. Removal of ground clutter

Detection of weak scatter is more easily compromised by ground clutter, thus we needed to implement a filter that strongly suppresses ground clutter. Toward this goal a notch filter centered on zero velocity and having a width of 4 m s^{-1} was applied. To avoid inadvertently filtering Bragg backscatter, data were collected in azimuth directions where airborne scatterers had radial velocities outside the notch. Although a 4 m s^{-1} wide notch should theoretically eliminate all ground clutter, spectral leakage, due to the large spectral sidelobes of the clutter signal samples, can cause clutter power to appear outside the notch as residues. For example, effects of such clutter residues can be seen in Fig. 2 within 4 km at elevation angles to 60°, and in the regions below 1 km where large negative and positive Z_{DR} values are seen. Furthermore, strong backscatter from ground objects at 0° elevation angle and beyond 4 km can be seen as high reflectivity factors (i.e., >20 dBZ) along the radar horizon (e.g., Fig. 2).

To avoid contamination of Bragg scatter echoes by ground clutter residues, polarimetric parameters have been measured beyond range of 5 km and above some

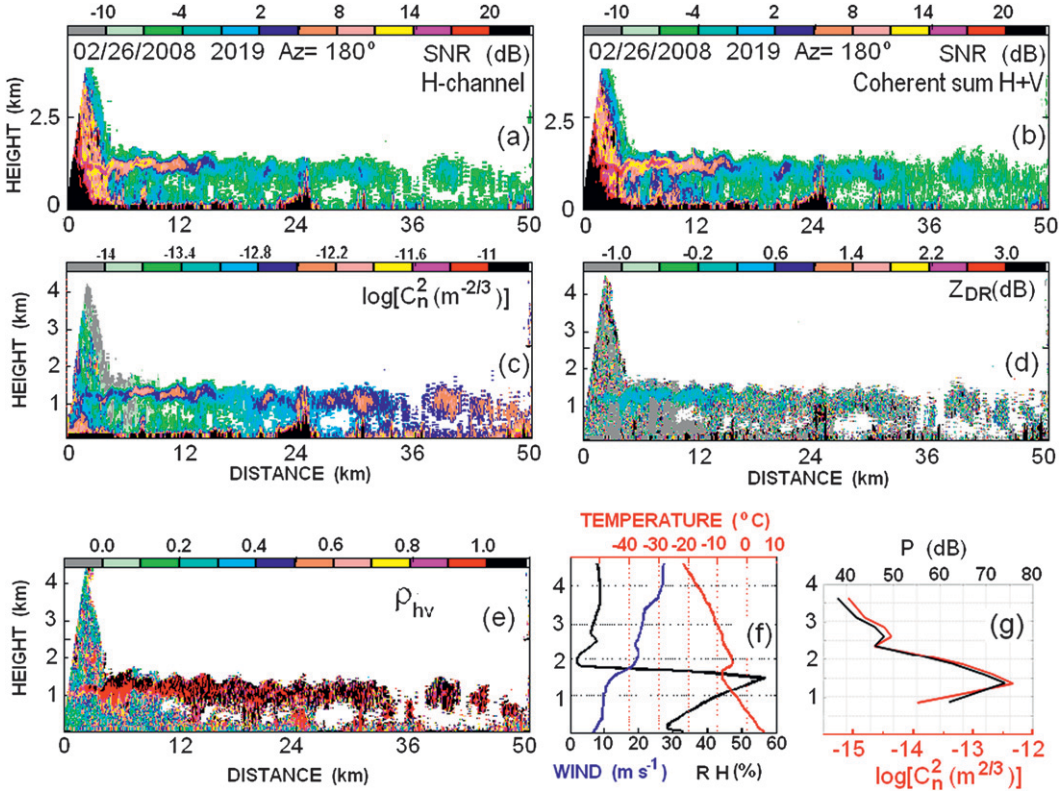

FIG. 2. Vertical cross sections of (a) SNR$_h$, (b) SNR$_{sum}$, (c) log(C_n^2), (d) Z_{DR}, and (e) ρ_{hv} fields. (f) Rawinsonde profiles of the temperature (red), wind speed (blue), and relative humidity (black) above Norman, OK, at 0000 UTC 27 Feb 2008. (g) Echo power P (black) and estimated log(C_n^2) (red) from the NPN profiler at Vici, OK, at 2018 UTC 26 Feb 2008. All data are presented above the radar horizon.

height below which ground clutter was evident. For each case presented herein, this height was obtained subjectively by inspecting the reflectivity fields. For instance, for the case in Fig. 2, this height was 0.5 km. (For other cases the heights are indicated in Fig. 4 above the panels.)

3. Selecting layers of Bragg scatter

In this section we discuss the methodology used to select regions of Bragg scatter so its polarimetric properties can be evaluated.

a. Distinguishing Bragg scatter from clutter due to biota

Using polarimetric radar, echoes from atmospheric biota can be distinguished from small water drop echoes because biota echoes typically have large positive Z_{DR} (dB) (Mueller and Larkin 1985; Wilson et al. 1994; Zrnic and Ryzhkov 1998; Lang et al. 2004). It is known that atmospheric biota have smaller correlation coefficients (i.e., $\rho_{hv} < 0.95$) compared to >0.98 for rain drops. If Bragg scatterers have Z_{DR} and ρ_{hv} properties similar to drizzle, as will be shown herein, these properties can then be used to distinguish Bragg and biota scatter under rain-free conditions.

In winter seasons, or for echo layer heights above the freezing level, it is assumed biota echoes are absent, and thus echoes are likely due to Bragg scatterers. For such layers, our observations show mean ρ_{hv} is larger than 0.98, and comparisons of vertical profiles of C_n^2 from KOUN and those obtained from a 74.3-cm wavelength profiler from the National Oceanic and Atmospheric Administration (NOAA) Profiler Network (NPN) show good agreement in altitudes of maximums of C_n^2 from the profiler and KOUN and reasonable agreement in the magnitude of C_n^2 when conditions of horizontally homogeneity apply (e.g., Figs. 2c,g). Profiler data are discussed more fully in section 3b. This comparison supports the premise that Bragg scatter is observed. In warm seasons, the boundary layer in Oklahoma is filled with biota. Sometimes layers of clear-air echoes are observed above the biota (e.g., Fig. 5). Using data from wind profilers, echoes from these elevated layers can more reliably be associated with Bragg scatter.

Because layers of Bragg scatter are often strongest where there are gradients of potential temperature and water

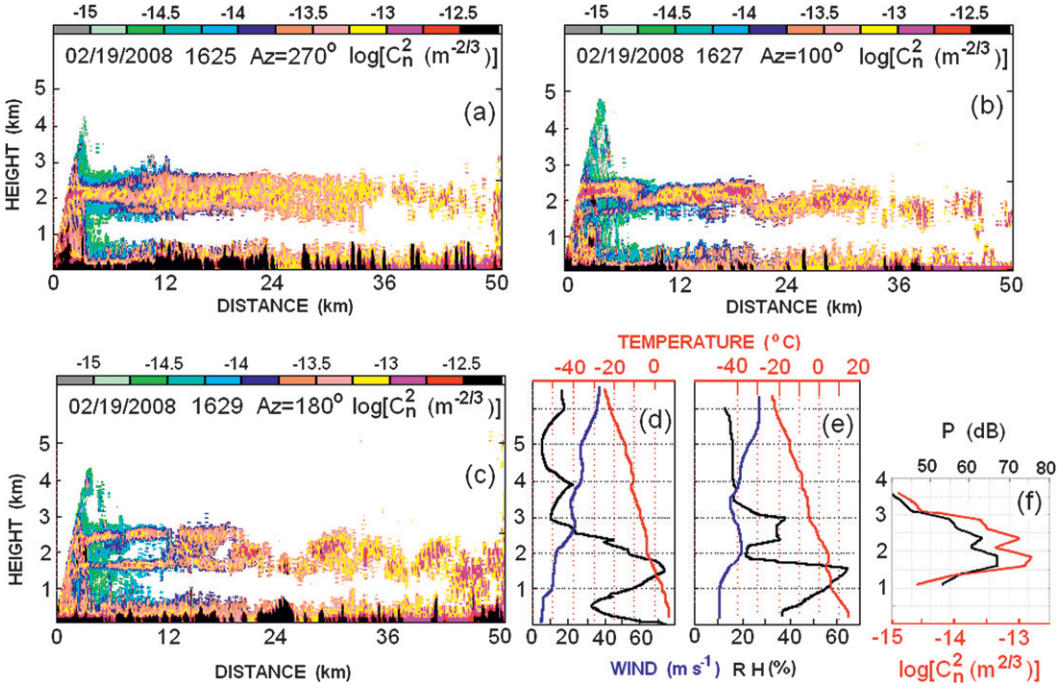

FIG. 3. (a),(b),(c) Vertical cross sections of $\log(C_n^2)$ at three azimuths. (d),(e) Rawinsonde profiles of the temperature, wind speed, and relative humidity at Norman, OK, at 1200 UTC 19 Feb and 0000 UTC 20 Feb 2008 embracing the time of radar observations. (f) Profiler data from the Purcell site as in Fig. 1.

vapor, rawinsonde data are also presented and examined to lend support for the selection of a layer of Bragg scatter.

This analysis suggests that to distinguish Bragg backscatter from biota clutter, data are needed to be acquired from those regions of the clear atmosphere that satisfy the following conditions:

1) Profiler data reveal peaks in the height profile of C_n^2 corresponding to peaks seen in the vertical cross sections of C_n^2 measured with KOUN.
2) Skies are cloud free.
3) Rawinsonde data show strong vertical gradients of water vapor/humidity.

These conditions have been applied to select layers where echoes are assumed to be exclusively from Bragg scatterers. Under these conditions, the polarimetric properties of Bragg scatterers can be determined. Condition 1) is the strongest, and if satisfied should insure by itself echoes are exclusively from Bragg scatterers. In some cases Bragg scatterers are imbedded in layers of biota and we apply polarimetric spectral analysis to identify regions of Bragg scatter (section 4b).

b. *Profiler and rawinsonde data*

All data fields derived from KOUN observations are accompanied with profiler data from the NPN site at Purcell, Oklahoma, located 29 km south-southwest from KOUN; the one exception is the NPN data (Fig. 2), which was not available from the Purcell site, so this data is from the NPN site at Vici, Oklahoma (187 km northwest from KOUN). In the profiler graphs, the signal power P is that measured with the vertical beam. Observations show that KOUN's echoes from Bragg scatter can be highly nonuniform spatially and temporally (Fig. 3). Data collected at three different azimuths show either a single echo layer near 2 km above ground level (AGL) with different thicknesses, or a two-layer echo pattern. Nevertheless, for the vertical cross section nearest the profile (i.e., Fig. 3c) both the profiler and radar show two layers of C_n^2 at nearly the same height and with the same order of magnitude. The profiler's returned powers are highly fluctuating in time. To reduce the variance in the profiler data, measurements ± 6 min around the time of KOUN observations were averaged. These data support the hypothesis that KOUN observes Bragg scatterers.

The rawinsonde observations show a very shallow CBL at 1200 UTC increasing to a depth of over 1700 m at 0000 UTC. Thermals from the surface would likely reach depths of above 2 km, as estimated from the potential temperature profile. Thus, the layer of maximum C_n^2 seen in the KOUN data appears to match the expected height of the CBL top, which also is the height with the strongest vertical moisture gradient. This result is

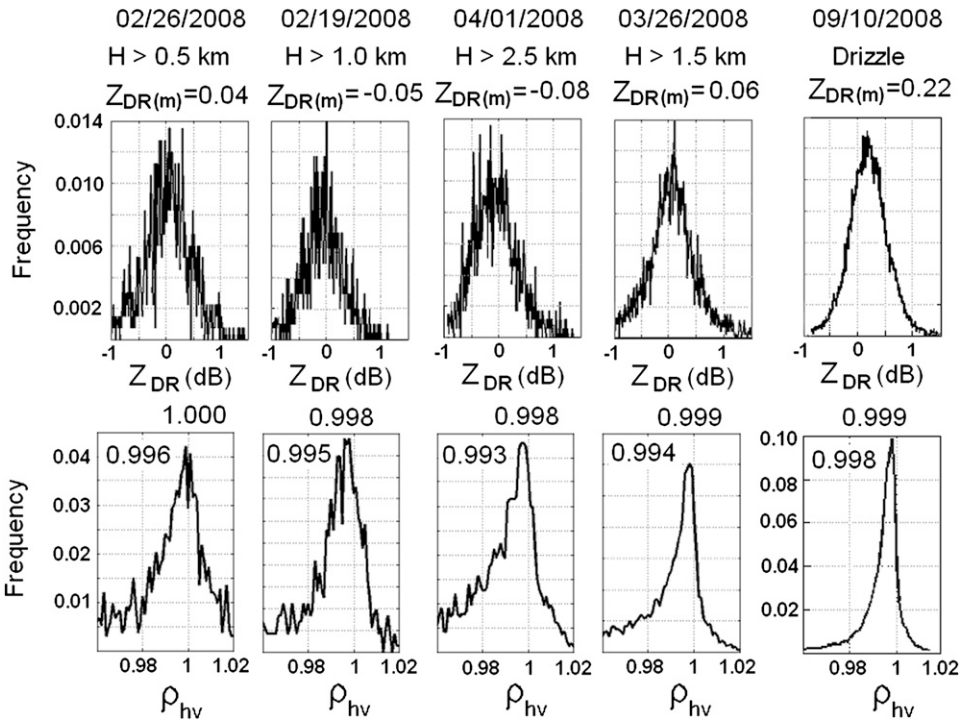

FIG. 4. Frequency of occurrences of (top) Bragg scatter Z_{DR} and (bottom) ρ_{hv} for (left to right) each observation. The last column is for drizzle with similar signal-to-noise ratios. Heights above which the data were analyzed are given below the observation dates; the $Z_{DR(m)}$ stands for the median value. Values of ρ_{hv} at the maxima of the histograms are presented at the tops of the ρ_{hv} plots, the values inside stand for the median values of ρ_{hv}.

consistent with both theory (Wyngaard and LeMone 1980; Fairall 1991) and observations (Oochs and Lawrence 1972) that indicate the value of C_n^2 peaks at the inversion on top of a CBL.

The NPN's principal goal is wind measurements. There is no strict monitoring of the profiler's radar constant as needed for quantitative reflectivity measurements as with KOUN for which this constant is monitored after each volume scan (i.e., every 5–6 min). To calculate C_n^2 from the profiler's echo power, the profiler's radar constant is needed. This constant was estimated by comparing KOUN and profiler precipitation reflectivity measured at the same time in rain. Then we used the profiler constant to calculate C_n^2. Estimated accuracy of the profiler's radar constant is ± 2 dB, which should be adequate for qualitative comparisons with KOUN's data. To quantitatively compare C_n^2 from radars with different wavelength, the radars should be well calibrated and sample exactly the same resolution volume (e.g., Hardy et al. 1966; Gage et al. 1980; Gossard 1981; Gossard and Strauch 1983; Gage et al. 1999). Neither of these conditions was met in our observations, and there was no attempt to make a quantitative comparison during the time the reported observations were made.

4. Polarimetric properties of Bragg scatterers

Maximal C_n^2 measured with KOUN in January–April 2008 was 2.5×10^{-12} m$^{-2/3}$. This agrees well with peak values of 3×10^{-12} m$^{-2/3}$ measured by Doviak and Berger (1980). In this section the measurements of Z_{DR} and ρ_{hv} properties for Bragg scatterers are presented. These properties can be useful in using a polarimetric radar to distinguish Bragg backscatter from those echoes associated with atmospheric biota.

a. Histograms of Bragg scatterers' polarimetric properties

Although the polarimetric properties of Bragg scatterers have not been previously reported, the value of Z_{DR} is expected to be 0 dB. This is so because the perturbations $\Delta N(\mathbf{r}, t)$ of the refractive index's scales that principally contribute to Bragg backscatter are 5 cm [i.e., half the radar wavelength; Doviak and Zrnic (2006), their section 11.4]. Such small scales are isotropic; that is, the spatial correlation function of $\Delta N(\mathbf{r}, t)$ at these scales is independent of direction of $\mathbf{r}$ (Doviak et al. 1996). Therefore the 5-cm-scale Bragg scatterers are spherically shaped in the mean and Z_{DR} should be 0 dB.

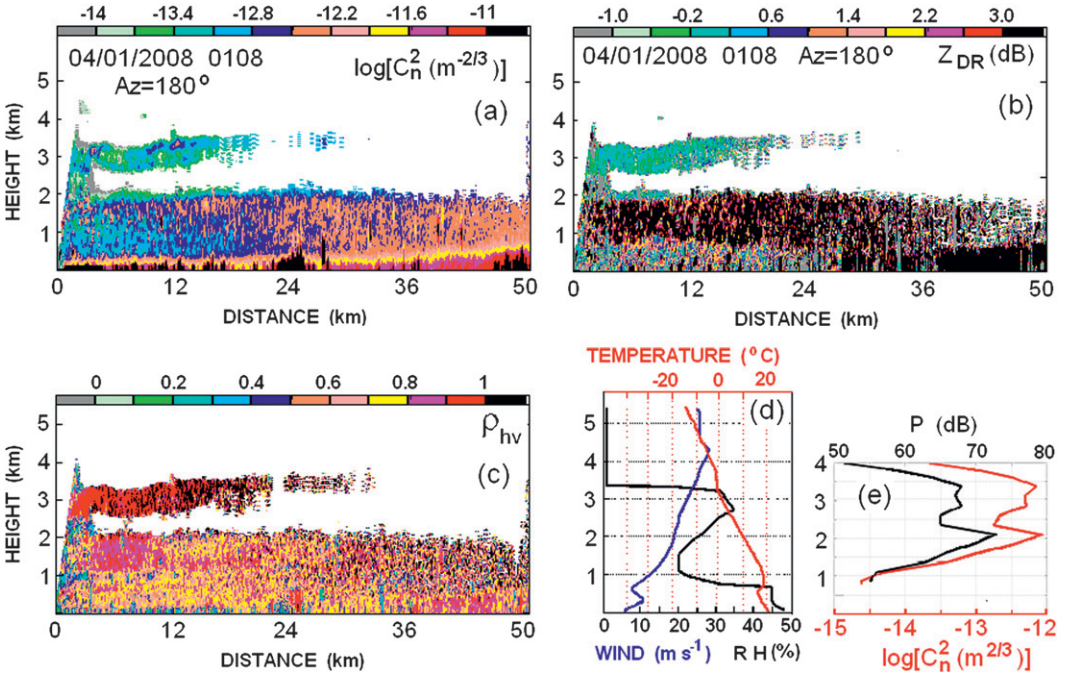

FIG. 5. As in Figs. 2c–g, but for data collected at 0108 UTC 1 Apr 2008. (d) Rawinsonde profiles are for 0000 UTC, and (e) P and C_n^2 profiles are from the NPN profiler at Purcell, OK.

An example of C_n^2, Z_{DR}, and ρ_{hv} fields from an elevated layer of supposed Bragg scatterers at the top of the CBL is shown in Fig. 2. As seen from the figure, values of Z_{DR} are close to 0 dB as expected, and values of ρ_{hv} are close to unity in the undulating layer of Bragg scatterers (i.e., at the height of 1.5 km). The enhanced reflectivity at 1.5 km is attributed to turbulence mixing moist and dry air (Doviak and Zrnic 2006, their sections 11.6 and 11.7). The system Z_{DR} has been monitored according to Zrnic et al. (2006) before and after clear-air observations so accuracy of the Z_{DR} measurements is ±0.1 dB. Thus, the span of the bluish green color category in Fig. 2d, one that embraces the expected Z_{DR} of Bragg scatterers, is chosen to be ±0.2 dB.

Because the visual observations showed no clouds, the temperature at the echo layer at 1.5 km is below freezing at −9°C (Fig. 2f), there is a strong vertical gradient of moisture at 1.5 km at the top of the CBL, and profiler data show a C_n^2 maximum at 1.5 km, it is concluded that the echoes at 1.5 km are Bragg scatter. Given that C_n^2 can vary by more than 10 times over a few kilometers (Fig. 2c), and KOUN measurements are more than 15 km from the profiler site, $\log(C_n^2)$ variations from about −13.6 to −12.2 (Fig. 2c) compare reasonably well with the profiler measured value of −12.3.

Bragg scatter reflectivity displayed in vertical cross sections are calculated using signals having SNR > −7 dB. But to obtain histograms of Z_{DR} and ρ_{hv} estimates, data with SNR > 5 dB have been used in all cases to eliminate large variations of estimates at lower SNR (Fig. 1). Frequencies of occurrences for Z_{DR} and ρ_{hv} estimates for the data in Fig. 2 are shown in the first column of Fig. 4. The measured median Z_{DR} is $Z_{DR(m)} = 0.04$ dB and $SD(Z_{DR}) < 0.2$ dB (Fig. 1). The distribution of ρ_{hv} is peaked at about 1.000, has a median value $\rho_{hv(m)} = 0.996$, is not symmetrical about 1.0, and has a more steep right side.

Distributions for drizzle observed with KOUN on 10 September 2008 are shown for comparison in the right column of Fig. 4. Drizzle data were selected in an area with similar SNR as for Bragg scatter. The median Z_{DR} is 0.22 dB (i.e., the drizzle contained some number of distorted droplets that produced slightly positive Z_{DR}). The distribution of ρ_{hv} in the drizzle is also not symmetrical and peaked at 0.999 with median value of 0.988. It is seen that the ρ_{hv} distributions for Bragg scatterers are wider than for drizzle. Bragg scatter data on other days are shown in columns 2–4.

Figure 5 presents a case of a layer of reflectivity at height of around 3 km in a cloud-free atmosphere, but above a layer of biota stretching from the ground up to 2 km; biota are distinguished by their large values of Z_{DR}. Because both the profiler and KOUN show a reflectivity layer at 3 km the upper layer is identified as a layer of Bragg scatterers. Rawinsonde data exhibit a strong gradient of relative humidity at heights around 3 km. The probability densities of Z_{DR} and ρ_{hv} for this layer of

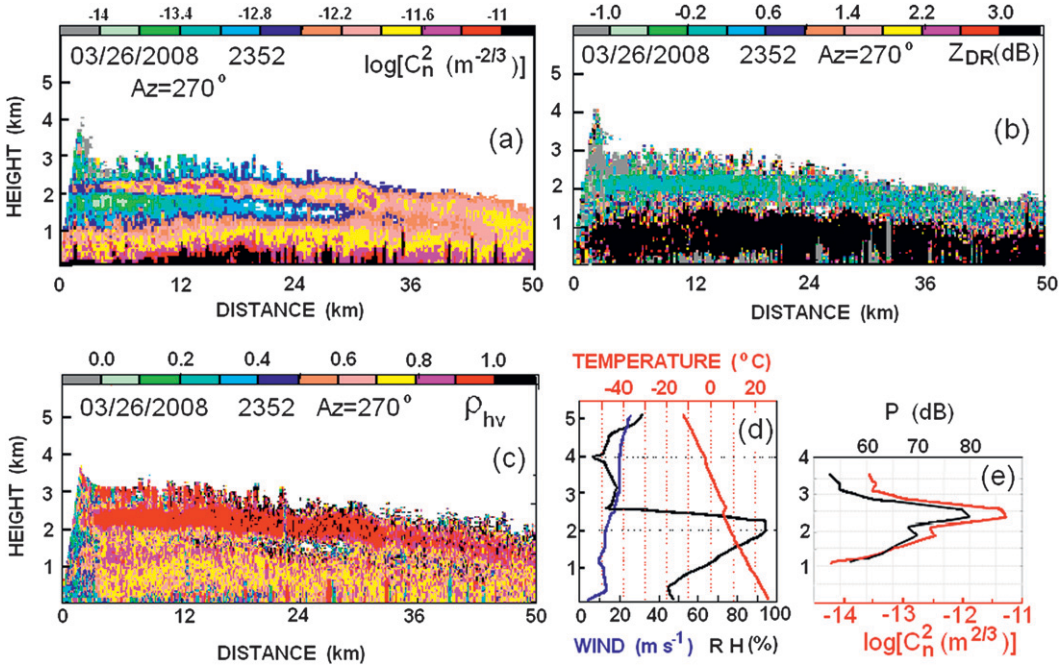

FIG. 6. As in Figs. 2c–g, but for data collected at 2352 UTC 26 Mar 2008. (d) Rawinsonde profiles are for 0000 UTC 27 Mar 2008.

Bragg scatterers are shown in the third column of Fig. 4. The Z_{DR} and ρ_{hv} estimates for this layer are spread around 0 and unity with medians of −0.08 dB and 0.993, respectively. The vertical profile of C_n^2 obtained from profiler data suggests two layers of Bragg scatter: one at 3.2- and the other at 2-km height (Fig. 5e). Although C_n^2 from KOUN data clearly show the Bragg scatter layer at 3.2-km height, echoes below 2 km from biota having large positive Z_{DR} mostly mask the Bragg scatter. Nevertheless, a thin layer of low Z_{DR} is seen at the height of 2 km; this could be evidence of Bragg scatter.

Another case of Bragg scatter is presented in Fig. 6 in which a Bragg scatter layer is seen sloping downward from a height of about 2.2 km above the radar to below 1.6 km above the radar horizon (i.e., ≈1.8 km AGL) at a range 50 km west. The Bragg scatter layer height above the radar agrees well with the height of the layer from the wind profiler. Rawinsonde data (Fig. 6d) showing a thick moist layer topped at 2.5 km confirms intense Bragg scatter. Thus, data suggest the moist layer is about 700 m shallower farther west. Below 1.2 km, the polarimetric data suggests the lower atmosphere is filled with biota because $Z_{DR} > +3$ dB. As noted by Zrnic and Ryzhkov (1998), this is the polarimetric characteristic of insects. There is good correspondence between the Bragg scatter layer height and the height of the strong gradient of relative humidity (Fig. 6d). Thus, it is likely that mixing of air at the steep gradient of moisture is creating intense C_n^2. Corresponding Z_{DR} and ρ_{hv} histograms are shown in the fourth column in Fig. 4.

Based upon data from all cases examined (summarized in Fig. 4), it is concluded that Bragg scatterers at 5-cm scales have $Z_{DR} \approx 0$ dB and $0.993 \leq \rho_{hv} \leq 1.0$. Thus, if sufficiently strong Bragg scatter can be confidently indentified with polarimetric radar, Bragg scatter can be used to check the system Z_{DR} bias of the WSR-88D. Echoes from Bragg scatterers should also give more reliable measurements of the radial velocity of wind without the bias as often is the case when biota are the scatterers in clear skies.

b. *Spectral analysis of mixed Bragg and biota scatter*

In warm seasons in Oklahoma, biota scatter frequently contaminates Bragg scatter. Under this condition distinguishing biota and Bragg scatter might be accomplished by analyzing the H and V Doppler spectra. If the atmospheric fauna are migrating, their velocities can significantly differ from the wind and consequently wind measurements will be severely biased if the fauna are strong fliers (e.g., birds). If, by using spectral analysis, fauna echoes can be distinguished from Bragg scatter, more accurate wind measurement could be made with polarimetric Doppler radar. Spectra or portions of the spectra associated with backscatter from biota should exhibit large differences in spectral power densities at horizontal and vertical polarizations whereas spectra or portions of the spectra

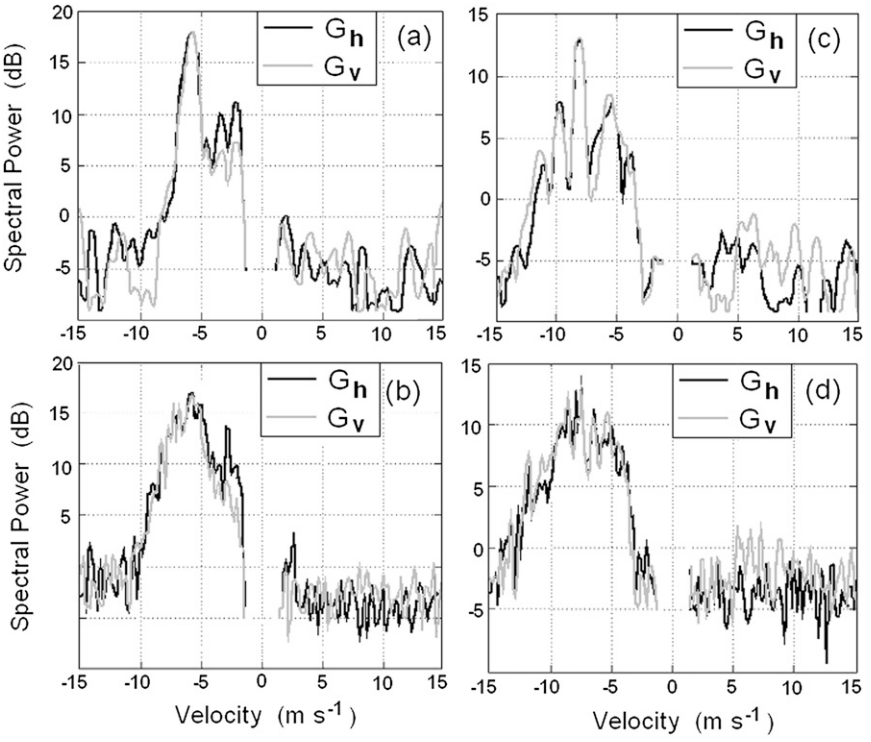

FIG. 7. Doppler spectra G_h and G_v for H and V polarizations for the case shown in Fig. 8. The antenna elevation is 3.1°. (a) The distance to radar volume for data is 19.75 km. (b) As in (a), but radially averaged over 10 range gates. (c),(d) As in (a),(b), but at the distance of 23.5 km.

associated with Bragg scatterers should have very small or negligible spectral power differences. Two such cases are presented in Fig. 7 for the same day as for the data shown in Fig. 6, but at an earlier time (i.e., 2049 UTC, Fig. 8) when the beam was pointing eastward. At this earlier time the layer of Bragg scatterers was lower (i.e., 1.5 km) and insects were present in the layer of Bragg scatterers. Echoes from two regions (shown in the ρ_{hv} panel in Fig. 8) are shown in Figs. 7a,c. Figures 7b,d depict the Doppler spectra of the regions each containing 10 resolution volumes. The von Hann weighting function was applied to the 256 samples of time series echo data that were collected and recorded during each dwell time from each resolution volume. To smooth spectral fluctuations, a 4-spectral line running average was performed and 10 spectra from each of the 2 regions were averaged to obtain the spectra shown in Figs. 7b,d. The total range in averaging was 1.25 km because resolution volumes were spaced 125 m apart.

In Fig. 7a, the Doppler spectra at the horizontal and vertical polarizations are shown for the range of 19.75 km, the height of the radar's resolution volume is 1.08 km. This volume is situated at the boundary of the layer with decreased Z_{DR} and increased ρ_{hv}. For the most part this spectrum is mostly associated with Bragg scatter because the spectral differential reflectivity [i.e., $Z_{DR}(v) \approx 0$ dB]. In the averaged spectrum in Fig. 7b, there is a narrow velocity interval between -2 and -4 m s^{-1}, where the spectral components have an integrated (i.e., spectral power density integrated over the interval) Z_{DR} of +3.9 dB. Thus, these spectral components are assumed to be associated with backscatter from insects and birds as suggested by Zrnic and Ryzhkov (1998). The total integrated $Z_{DR} = 0.54$ dB.

Figure 7c presents the Doppler spectra inside the layer with decreased Z_{DR} and increased ρ_{hv} (i.e., further into the layer of supposed Bragg scatter). The distance to the radar volume was 23.5 km with the height of 1.3 km. In this case there are no spectral lines with significant differential reflectivities, suggesting these spectra are principally associated with Bragg scatter. If biota are fast-migrating birds, there is the possibility that Bragg scatter spectra could be separated from the spectra associated with biota (i.e., there would be two distinct spectral peaks).

5. Discussion and conclusions

Observations with a dual-polarization WSR-88D (KOUN) show the capability to measure C_n^2 as low as 3.5×10^{-15} m$^{-2/3}$ at a range of 10 km; this is about

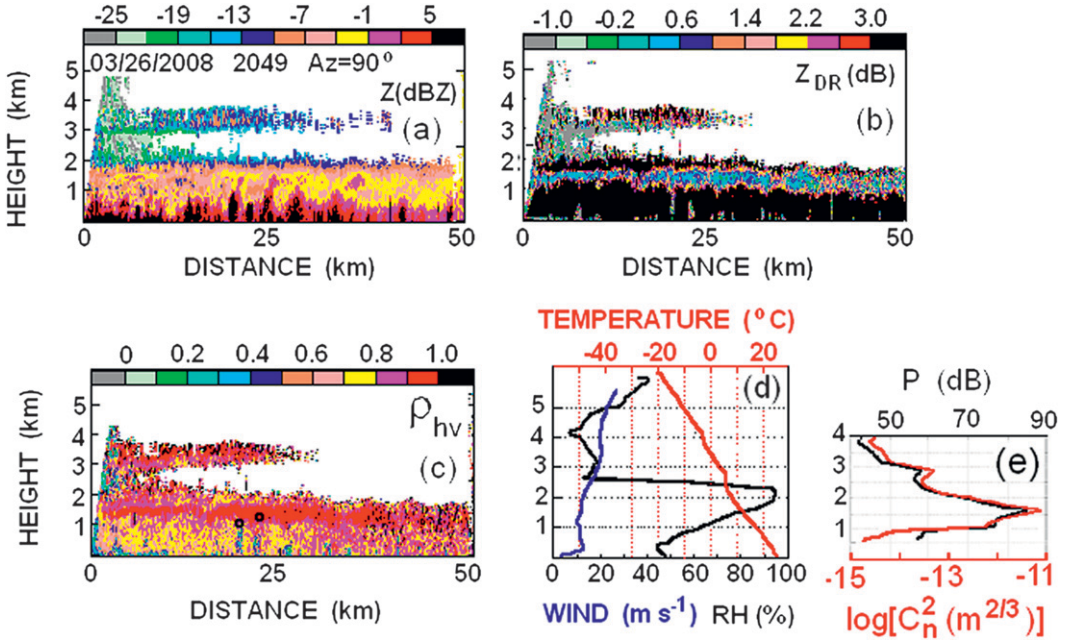

FIG. 8. Polarimetric and profiler data for the same day as presented in Fig. 6, but about 3 h earlier, and with the beam directed eastward with format as in Fig. 8. The two black circles in the ρ_{hv} plot mark regions from which received echoes were spectrally analyzed. (a) The reflectivity factor Z(dBZ) field is shown instead of $\log(C_n^2)$ because the echo is dominated by reflections from insects.

two orders of magnitude below the mean C_n^2 of 5×10^{-13} m$^{-2/3}$ measured with an airborne refractometer in maritime boundary layer air over Oklahoma (Doviak and Berger 1980). Observations with KOUN show significant advantage of having a scanning capability to map the horizontal extent and structure of C_n^2. In cases where ''clear air'' returns to KOUN are thought not to have been contaminated with airborne biota clutter, a good correspondence was found between the properties of echo layers observed with KOUN and with longer wavelength wind profilers. Thus, the NPN profiler and WSR-88D networks have the potential to provide, by working in a coordinated approach, more reliable meteorological data.

Maximal C_n^2 measured with KOUN from January to April 2008 was 2.5×10^{-12} m$^{-2/3}$. This agrees markedly well with peak values of 3×10^{-12} m$^{-2/3}$ measured by Doviak and Berger (1980) with a 10-cm wavelength radar for maritime air over Oklahoma.

Medium differential reflectivities of Bragg scatterers, using enhanced data collection and processing procedures on KOUN, lie in the interval -0.08 to 0.06 dB. Thus, it is concluded that Bragg scatter at 10-cm wavelengths has $Z_{DR} \approx 0$ dB; this is as expected based on theoretical grounds (section 4a). The distributions of the measured Bragg scatter correlation coefficients ρ_{hv} have peaks between 0.998 and 1.0 with a median value of 0.995. Having ρ_{hv} so close to 1.000 confirms the good polarimetric quality of the WSR-88D's antenna for polarimetric measurements. The intrinsic 0 dB of Bragg scatter can be used for verifying of Z_{DR} radar calibration.

Layers of Bragg scatterers have also been observed within layers of biota. In some such cases slightly positive Z_{DR} (0.2–0.3 dB) and decreased ρ_{hv} (as low as 0.977 for the median value) are attributed to the presence of biota. In one case a layer of Bragg scatter was present at the top of the CBL, with biota both below and above. But, as shown (section 4b), polarimetric spectral analysis has the potential to better distinguish the two types of scatterers, even when both are present within the radar's resolution volume.

Because Bragg scatter $Z_{DR} \approx 0$ dB and $\rho_{hv} \approx 1$, coherent summation of signals from the H and V receiver channels can add as much as 3 dB to the signal-to-noise ratio, thus enhancing radar capability to observe Bragg scatter. This could enlarge the area of radar measurement and/or reduce the standard deviations of C_n^2 and Doppler velocity estimates.

Results suggest that one potential meteorological application of Bragg scatter mapping is monitoring the temporal and spatial changes in the depth of the CBL. Detection of the CBL top is likely more reliable if the upper boundary of CBL is being mixed by strong turbulence as is so often the case when daytime surface heating creates thermal plumes. Furthermore, results show that

the NPN wind profiler and WSR-88D weather radar networks have the potential to provide, by working in a coordinated approach, a more reliable measure of the top of the CBL. However, much more routine data collection is needed to establish the reliability of this approach throughout the daytime portion of the diurnal cycle, during partly cloudy and cloudy conditions, during all seasons of the year, and across a spectrum of different environmental conditions. It is encouraging that Heinselman et al. (2009a) have used the nonpolarimetric WSR-88D to measure CBL height and suggested polarimetric radar might better distinguish Bragg scatter to obtain a more reliable method to monitor the depth of the CBL. It could be that the Heinselman et al. (2009a) approach could also be combined with Bragg scatter detection and NPN wind profiler data to yield an even more reliable CBL depth observation. Given that the WSR-88D can be used to monitor the temporal and spatial changes of water vapor near the earth using backscatter from fixed ground objects, additional information on the depth of the CBL from a polarimetric WSR-88D could provide an important constraint on the changes in water vapor, pollutants, and turbulence within the boundary layer. This combined information would be valuable to forecasters concerned about convection initiation and evolution, air quality, hazardous releases, and wildfires, and could be used in the initialization of rapidly updating numerical weather prediction models. Current model predictions of CBL depth often differ from observations by a factor of 2 (Bright and Mullen 2002; Stensrud and Weiss 2002), suggesting that estimates of CBL depth would provide new information that could be used advantageously in data assimilation systems. Convective boundary layer depth observations would also allow forecasters to assess the model forecasts of CBL depth and alter their expectations of moisture depth, convective inhibition, and instability, thereby improving forecasts of the timing and likelihood of storm initiation.

Acknowledgments. We thank Dr. R. Rabin for the discussion on the topics and Dr. D. van de Kamp for his comments on wind profiler's operations. Funding for this study was provided by the NOAA/Office of Oceanic and Atmospheric Research under NOAA–University of Oklahoma Cooperative Agreement NA17RJ1227 (U.S. Department of Commerce).

REFERENCES

Bachmann, S., and D. Zrnic, 2007: Spectral density of polarimetric variables separating biological scatterers in the VAD display. *J. Atmos. Oceanic Technol.,* **24,** 1186–1198.

Bodine, D., P. Heinselman, B. Cheong, R. Palmer, and D. Michaud, 2010: A case study on the impact of moisture variability on convection initiation using radar refractivity retrievals. *J. Appl. Meteor. Climatol.,* **49,** 1766–1778.

Bright, D. R., and S. L. Mullen, 2002: Short-range ensemble forecasts of precipitation during the Southwest monsoon. *Wea. Forecasting,* **17,** 1080–1100.

Doviak, R. J., and M. J. Berger, 1980: Turbulence and waves in the optically clear planetary boundary layer resolved by dual Doppler radars. *Radio Sci.,* **15,** 297–317.

——, and D. S. Zrnic, 2006: *Doppler Radar and Weather Observations*. 2nd ed. Dover Publications, 562 pp.

——, R. J. Lataitis, and C. L. Holloway, 1996: Cross correlations and cross spectra for spaced antenna wind profilers. Part 1: Theoretical analysis. *Radio Sci.,* **31,** 157–180.

——, V. Bringi, A. Ryzhkov, A. Zahrai, and D. Zrnic, 2000: Considerations for polarimetric upgrades to operational WSR-88D radars. *J. Atmos. Oceanic Technol.,* **17,** 257–278.

Fabry, F., 2006: The spatial structure of moisture near the surface: Project-long characterization. *Mon. Wea. Rev.,* **134,** 79–91.

——, C. Frush, I. Zawadzki, and A. Kilambi, 1997: On the extraction of near-surface index of refraction using radar phase measurements from ground targets. *J. Atmos. Oceanic Technol.,* **14,** 978–987.

Fairall, C. W., 1991: The humidity and temperature sensitivity of clear-air radars in the convective boundary layer. *J. Appl. Meteor.,* **30,** 1064–1074.

Gage, K. S., J. L. Green, and T. E. VanZandt, 1980: Use of Doppler radar for the measurement of atmospheric turbulence parameters from the intensity of clear air echoes. *Radio Sci.,* **15,** 407–416.

——, C. R. Williams, W. L. Ecklund, and P. E. Johnston, 1999: Use of two profilers during MCTEX for unambiguous identification of Bragg scattering and Rayleigh scattering. *J. Atmos. Sci.,* **56,** 3679–3691.

Gossard, E. E., 1981: Clear weather meteorological effects on propagation at frequencies above 1 GHz. *Radio Sci.,* **6,** 589–608.

——, and R. G. Strauch, 1983: *Radar Observations of Clear Air and Clouds*. Elseiver, 280 pp.

Hardy, K. R., D. Atlas, and K. M. Glover, 1966: Multiwavelength backscatter from the clear atmosphere. *J. Geophys. Res.,* **71,** 1537–1552.

Heinselman, P., B. L. Cheong, R. D. Palmer, D. Bodine, and K. Hondl, 2009a: Radar refractivity retrievals from KTLX: Insights in operational benefits and limitations. *Wea. Forecasting,* **24,** 1345–1361.

——, D. J. Stensrud, R. M. Hluchan, P. L. Spencer, P. C. Burke, and K. L. Elmore, 2009b: Radar reflectivity–based estimates of mixed layer depth. *J. Atmos. Oceanic Technol.,* **26,** 229–239.

Holleman, I., H. van Gasteren, and W. Bouten, 2008: Quality assessment of weather radar wind profiles during bird migration. *J. Atmos. Oceanic Technol.,* **25,** 2188–2198.

Lang, T. J., S. A. Rutledge, and J. L. Smith, 2004: Observations of quasi-symmetric echo patterns in clear air with the CSU-CHILL polarimetric radar. *J. Atmos. Oceanic Technol.,* **21,** 1182–1189.

Mahrt, L., 1977: Influence of low-level environment on severity of High-Plains moist convection. *Mon. Wea. Rev.,* **105,** 1315–1329.

Melnikov, V. M., and D. S. Zrnic, 2007: Autocorrelation and cross-correlation estimators of polarimetric variables. *J. Atmos. Oceanic Technol.,* **24,** 1337–1350.

——, and P. T. Schlatter, 2011: Enhancing sensitivity on the polarimetric WSR-88D. Preprints, *27th Conf. on Interactive Information Processing Systems (IIPS),* Seattle, WA, Amer. Meteor. Soc., 14.3. [Available online at http://ams.confex.com/ams/91Annual/webprogram/Paper178856.html.]

——, D. S. Zrnic, R. J. Doviak, P. B. Chilson, D. B. Mechem, and Y. L. Kogan, 2011: Prospects of the WSR-88D radar for cloud studies. *J. Appl. Meteor. Climatol.,* **50,** 859–872.

Moran, K. P., B. E. Martner, M. J. Post, R. A. Kropfli, D. C. Welsh, and K. B. Widener, 1998: An unattended cloud profiling radar for use in climate research. *Bull. Amer. Meteor. Soc.,* **79,** 443–455.

Mueller, E. G., and R. P. Larkin, 1985: Insects observed using dual-polarization radar. *J. Atmos. Oceanic Technol.,* **2,** 49–54.

National Research Council, 1998: *The Atmospheric Sciences: Entering the Twenty-First Century*. National Academies Press, 384 pp.

Oochs, G. R., and R. S. Lawrence, 1972: Temperature and Cn2 profiles measured over land and ocean to 3 km above the surface. NOAA Tech Rep. ERL 251-WPL 22, NOAA/Environmental Research Laboratories, Boulder, CO, 39 pp.

Ottersen, H., 1969: Atmospheric structure and radar backscattering in clear air. *Radio Sci.,* **4,** 1179–1193.

Roberts, R. D., and Coauthors, 2008: REFRACTT 2006. *Bull. Amer. Meteor. Soc.,* **89,** 1535–1548.

Stensrud, D. J., and S. J. Weiss, 2002: Mesoscale model ensemble forecasts of the 3 May 1999 tornado outbreak. *Wea. Forecasting,* **17,** 526–543.

Ulaby, F. T., R. K. Moore, and A. K. Fung, 1986: *Microwave Remote Sensing: Active and Passive*. Book-Mart Press, 2162 pp.

Wilczak, J. M., and Coauthors, 1995: Contamination of wind profiler data by migrating birds: Characteristics of corrupted data and potential solutions. *J. Atmos. Oceanic Technol.,* **12,** 449–467.

Wilson, J. W., T. M. Weckwerth, J. Vivekanandan, R. M. Wakimoto, and R. W. Russel, 1994: Boundary layer clear-air radar echoes: Origin of echoes and accuracy of deriving winds. *J. Atmos. Oceanic Technol.,* **11,** 1184–1206.

Wyngaard, J. C., and M. A. LeMone, 1980: Behavior of the refractive index structure parameter in the entraining convective boundary layer. *J. Atmos. Sci.,* **37,** 1573–1585.

Zrnic, D. S., and A. V. Ryzhkov, 1998: Observations of insects and birds with a polarimetric radar. *IEEE Trans. Geosci. Remote Sens.,* **36,** 661–668.

——, V. M. Melnikov, and J. K. Carter, 2006: Calibrating differential reflectivity on the WSR-88D. *J. Atmos. Oceanic Technol.,* **23,** 944–951.